

Photoreflectance spectroscopy with white light pump beam

Sandip Ghosh and B. M. Arora

Solid State Electronics Group, Tata Institute of Fundamental Research, Colaba, Mumbai-400 005, India

(Received 20 June 1997; accepted for publication 2 December 1997)

Using a dual chopping scheme where both the pump beam and the probe beam are chopped, we show that it is possible to perform photoreflectance spectroscopy with a broadband white light source as the pump beam instead of a laser source. We show that although the signal strength is reduced by a factor of $1/\pi$ in the dual chopping scheme, it nevertheless has several advantages. A white light pump beam provides a wide range of excitation energy values, enabling one to characterize semiconductors of different band gaps spread over a wide energy range with a single modulation source. In the case of semiconductor heterostructures, simultaneous as well as selective excitation of different interfaces can be achieved easily. This technique is not plagued by the problem of background due to luminescence often encountered in low-temperature photoreflectance measurements. In this article, we present the details of this technique and demonstrate its usefulness by applying it to selected semiconductor heterostructure samples. © 1998 American Institute of Physics. [S0034-6748(98)00503-6]

I. INTRODUCTION

In recent years, nondestructive electromodulation techniques of photoreflectance (PR)^{1,2} and contactless electroreflectance (CER)³ spectroscopy have gained considerable popularity as tools for the study and characterization of semiconductors and their heterostructures.^{4,5} Of the two, PR is a relatively simpler technique, however, CER has an advantage over PR in that the latter is plagued by the problem of high background due to scattered pump light and luminescence at low temperatures. Furthermore, in CER it is possible to simultaneously modulate the reflectivity at the interfaces between various layers of a heterostructure sample with different band gaps, thereby enabling the characterization of the whole structure. In a conventional PR measurement, with a fixed pump beam wavelength, this may not always be possible, particularly if the pump light is absorbed in a top layer and the excited carriers are unable to reach the interfacial regions lying underneath or if the pump beam photons do not have sufficient energy to excite carriers. A common problem often encountered in the analysis of the spectra of heterostructures is that of separating signals corresponding to various layers, which may overlap or lie close together. Similarly, it is difficult to distinguish signals from the two interfaces of a layer. It is here that PR can have an edge over CER if it should be possible to separately excite carriers in selected layers of a multilayered sample and thereby separate signals from different interfaces/layers. In a conventional PR experiment, selective modulation of various interfaces with a fixed wavelength pump beam source is difficult to achieve as a pump beam wavelength suitable for generating carriers in one of the layers of the heterostructure sample may not be suitable for another. To address this problem, use has been made of different laser pump beam sources.⁶ Pump wavelength tunability has also been achieved by using a high-power xenon lamp in combination with a second monochromator as the pump beam source.⁷ Measurement techniques such as differential photoreflectance⁸ have been proposed.

However, an easy solution to this problem can be achieved if it were possible to use a white light source as the pump beam with ordinary colored glass filters for selecting the required broadband pump beam wavelength range. In the case of heterostructure samples where signals from the various layers do not merge together, the use of a white light pump beam should make it possible to simultaneously modulate all the interfaces and characterize all the layers at one go. Thus, the use of a white light pump beam in photoreflectance spectroscopy can provide simultaneous as well as selective excitation of different interfaces of a heterostructure sample. In conventional PR spectroscopy, it is not possible to use a white light source as the pump beam for reasons discussed below. We have been able to solve this problem by adopting the dual chopped photoreflectance (DCPR) technique described below.

II. DUAL CHOPPED PHOTOREFLECTANCE

This technique was originally used by Lu *et al.*⁹ to overcome the problem of the scattered pump laser beam in photoreflectance spectroscopy. Thereafter Chandler-Horowitz *et al.*¹⁰ and independently Ghosh and Arora¹¹ have used it to overcome the problem of luminescence that is encountered at low temperatures in photoreflectance spectroscopy. Chandler-Horowitz *et al.* suggested that the signal strength in the dual chopping scheme is reduced by a factor of $1/2$, however, our analysis detailed below shows that it is not so.

In a conventional PR measurement the pump laser beam is chopped at a frequency f_1 (angular frequency $\omega_1 = 2\pi f_1$), which modulates the reflectivity of the sample at that frequency. The chopped laser beam has a near-rectangular wave form, but in our analysis we shall only consider its first Fourier component onto which the lock-in amplifier (LIA) locks on. The time-dependent reflectivity of the sample, due to the periodic modulation of the electric field at an interface by the pump laser beam, is a function of the incident probe beam photon energy E , and is then given by

$$R_s(E) = R_{s0}(E) + \frac{2}{\pi} \Delta R_s(E) \sin(\omega_1 t), \quad (1)$$

where $R_{s0}(E)$ is the reflectivity of the sample in the absence of the pump beam. $\Delta R_s(E)$ is the amplitude of the change in reflectivity due to the modulation. We have neglected the other dc term $[= \Delta R_s(E)/2]$ in Eq. (1) as it is much smaller than $R_{s0}(E)$. The probe beam intensity is dc and so the signal S_1 from the detector will be given by

$$S_1 = I_0(E)R_{s0}(E) + \frac{2}{\pi} I_0(E)\Delta R_s(E)\sin(\omega_1 t), \quad (2)$$

where $I_0(E)$ is the probe beam intensity and includes the measurement system's response to the incident photon energy including that of the lamp, the monochromator, the optics, and the detector. Thus, if one locks on to the frequency f_1 , one can measure a signal proportional to $(2/\pi)I_0(E)\Delta R_s(E)$. Then, dividing this spectrum by the simple reflectivity spectrum $(2/\pi)I_0(E)R_{s0}(E)$, one gets the required PR spectrum in the form of $\Delta R_s/R_{s0}$ as a function of energy. Now, the problem with this technique is that the pump light (laser) scattered from the sample surface reaching the detector is chopped at the same frequency (f_1) at which the lock-in detects the signal. Typically, the PR signals are in the μV range while the scattered pump beam strength depends on the surface quality of the sample and can be as high as a few mV. Therefore, the PR signal is completely swamped by the scattered pump beam reaching the detector. To overcome this problem, a long (wavelength) pass optical filter is placed in front of the detector to cut off the scattered pump beam light. This, in turn, means that all the spectral features at wavelengths shorter than the cutoff of the optical filter (or in the region around the pump beam wavelength if a bandpass filter were used) are lost. So, if a broadband white light pump beam source was used in the place of a laser source, the above would translate to the whole spectrum being lost. To overcome this problem we have adopted the dual chopped photoreflectance technique, wherein both the pump and the probe beam are chopped at frequencies f_1 and f_2 , respectively. The probe beam is now a near-rectangular wave form and considering its first harmonic, the signal S_2 from the detector will be given by

$$S_2 = \frac{2}{\pi} I_0(E) \sin(\omega_2 t + \phi) \times R_s(E), \quad (3)$$

where ϕ is the phase difference between the first harmonic of the ac component of reflectivity and that of the probe beam at $t=0$. Upon expansion using Eq. (1), Eq. (3) becomes

$$\begin{aligned} S_2 = & \frac{2}{\pi} I_0(E) R_{s0}(E) \sin(\omega_2 t + \phi) \\ & + \frac{2}{\pi^2} I_0(E) \Delta R_s(E) \cos[(\omega_1 + \omega_2)t + \phi] \\ & + \frac{2}{\pi^2} I_0(E) \Delta R_s(E) \cos[(\omega_1 - \omega_2)t - \phi]. \end{aligned} \quad (4)$$

Thus, if in-phase detection is made at a frequency $f_1 + f_2$ ($f_1 - f_2$ will have larger $1/f$ noise), which is synthesized

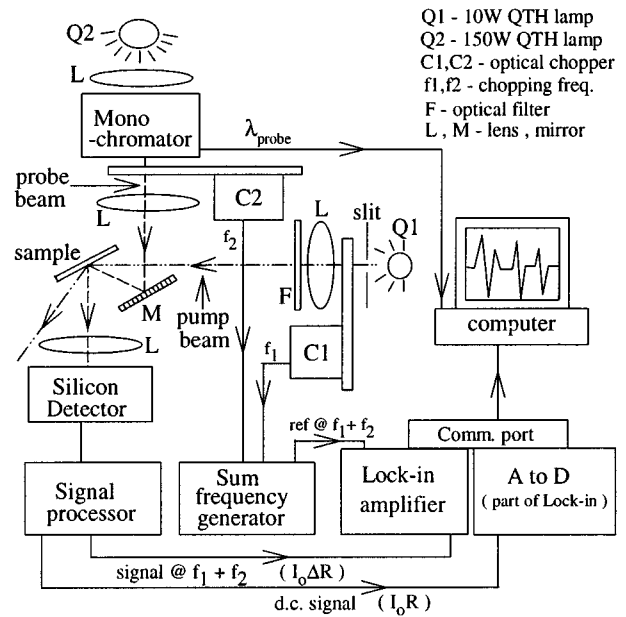


FIG. 1. Schematic of the experimental setup.

from the outputs of the two choppers that chop the pump and the probe beam, then one can measure a signal proportional to $(2/\pi^2)I_0(E)\Delta R_s(E)$. However, since the LIA is no longer locked onto the frequency f_1 at which the scattered pump beam signal arises, it no longer hampers our measurement and we can do away with the long (wavelength) pass filter used to block the scattered pump beam. This, in turn, allows us to use a wideband white light source as the pump beam for photoreflectance (WLPR) measurements. As before, dividing this spectrum by a $(2/\pi)I_0(E)R_{s0}(E)$ spectrum we get a $1/\pi(\Delta R_s/R_{s0})$ spectrum as a function of energy. We, therefore, find that the signal in a DCPR spectrum is $1/\pi$ times that in a conventional PR spectrum. This has been experimentally verified earlier¹¹ and it contradicts the suggestion of Chandler-Horowitz *et al.* who claimed that the reduction factor was $1/2$. Also, at low temperatures the pump beam excites luminescence in the sample, which for good quality samples is much larger than the PR signal, and like the scattered pump beam has a periodicity f_1 and, therefore, swamps the PR signal in a conventional single chopping experiment. In this case, one cannot even use an optical filter to cutoff the luminescence as it occurs in the same spectral region where we expect the PR signature to be. However, it is clear from the preceding analysis that the DCPR technique will not be hampered by the luminescence problem, a fact which has been shown earlier through experiments.⁹⁻¹¹

III. EXPERIMENTAL DETAILS

Figure 1 shows a schematic of the experimental setup. The pump beam is obtained by passing the light from a 10 W quartz-tungsten-halogen (QTH) lamp through a slit and is focused to a spot size of $0.8 \text{ mm} \times 2 \text{ mm}$ on the sample. It is chopped at frequency $f_1 (= 139 \text{ Hz})$ by chopper C1. The pump beam spectrum is shown in Fig. 4(c). The probe beam is obtained by dispersing light from a 150 W QTH lamp using a 1/8 m monochromator. It is chopped at frequency

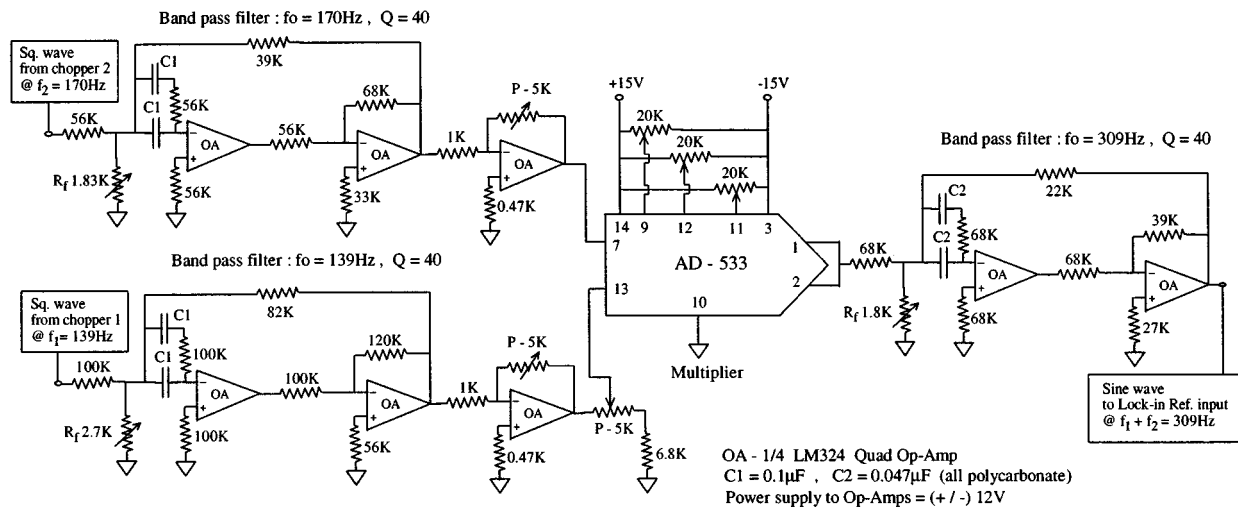


FIG. 2. Circuit diagram of the sum-frequency generator.

$f_2 (= 170 \text{ Hz})$ by chopper C2. The sum-frequency generator synthesizes a sinewave at frequency $f_1 + f_2 (= 309 \text{ Hz})$, using the outputs from the two chopper controllers. Lu *et al.*⁹ did not give any details of the circuits used by them to generate the sum frequency while Chandler-Horowitz *et al.*¹⁰ did do so. Our circuit for generating the sum frequency is different from that of Chandler-Horowitz *et al.* in that while they used passive $L-C$ filters and exploited the nonlinear characteristics of a junction field effect transistor (JFET) for signal multiplication, we have used active $R-C$ filters and an integrated circuit multiplier chip for signal multiplication. The sum-frequency generator circuit is shown in Fig. 2. It consists of two bandpass filters at the input stage tuned ($Q \approx 40$) at f_1 and f_2 , which pick out the first harmonics of the input rectangular reference wave forms from the two chopper controllers and amplifies them. The resistors R_f can be adjusted to fine tune the peak response frequency of these circuits. The design equations for determining the component values can be found in Ref. 12. The amplified sinewave out-

puts from these two filters are then fed to an analog four-quadrant multiplier, which in the present case is the chip AD-533 from Analog Devices. The output of the multiplier is filtered by another bandpass filter tuned at $f_1 + f_2$, which passes this component and blocks the $f_1 - f_2$ component. The output at $f_1 + f_2$ is fed as reference to the lock-in amplifier.

The signal from the silicon photodiode detector has the following main components (i) a square wave (at f_1), whose amplitude is proportional to the sum of the scattered pump beam intensity and the luminescence (at low temperatures) intensity (\approx few mV); (ii) a square wave (at f_2), whose amplitude is proportional to the reflected probe beam intensity (\approx few hundred mV); and (iii) harmonics at $f_1 + f_2$ and $f_1 - f_2$ (and others at the sum and difference of the multiples of f_1 and f_2), whose amplitudes are proportional to the change in the reflected probe beam intensity due to the periodically modulated reflectivity of the sample (\approx few tens of μV). Although the large ac signals at frequencies f_1 and f_2 are not

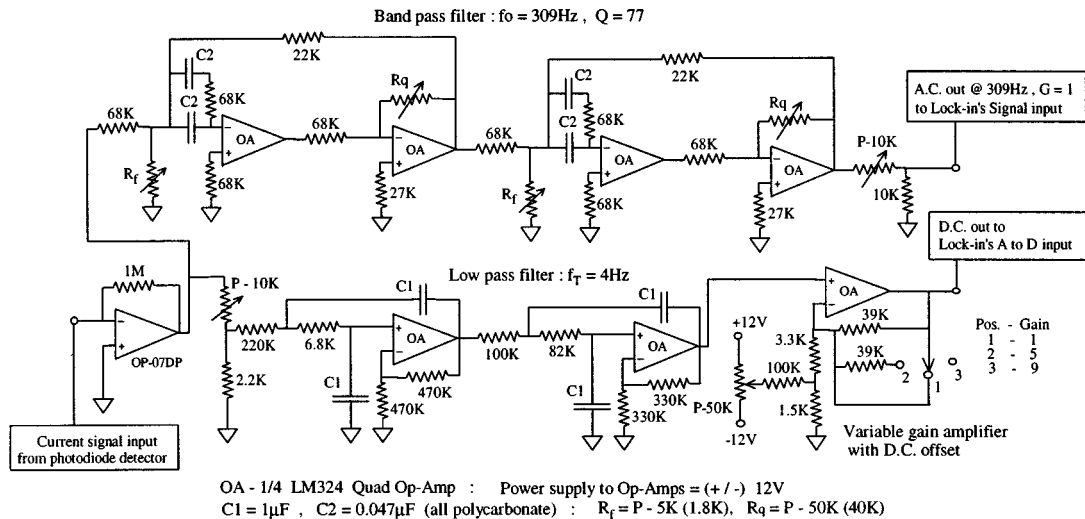


FIG. 3. Circuit diagram of the signal processor.

detected by the LIA, which is locked at $f_1 + f_2$, they nevertheless saturate the input amplifier of the LIA and add to the noise, thus preventing the measurement of the small signal at $f_1 + f_2$. This necessitates passing the signal from the detector through a signal processor before the signal is fed to the LIA. The signal processor circuit shown in Fig. 3 has two parts. After the current signal from the detector is converted to a voltage signal it is fed to two channels. The first one has a bandpass filter tuned at $f_1 + f_2$ ($Q \approx 77$). It passes the signal proportional to $I_0(E)\Delta R_s(E)$, which is then measured by the LIA. The resistors R_f and R_q can be adjusted to fine tune the peak response frequency and Q , respectively, of this circuit. The second channel has a low-pass filter, which outputs the average dc signal from the detector after suitable amplification. We make use of the fact that the square-wave signal at f_2 whose amplitude is proportional to $I_0(E)R_s(E)$, is by far the largest and has an average dc value proportional to the amplitude of the square wave. Therefore, the average dc signal directly gives a measure of $I_0(E)R_s(E)$, which is then read via one of the analog-to-digital conversion inputs provided as an added facility in most modern LIA. The design equations for determining the component values of the filter circuits can be found in Ref. 12. However, the filtered dc part also has a contribution (relatively small in comparison to the main signal due to the probe beam) from the scattered pump beam, which we do not want. But since the pump beam wavelength is not changed during a measurement, therefore, it gives rise to a constant background. In order to record this constant background, we switch on only the pump beam and not the probe beam before the start of the measurement. The dc reading under these conditions gives the magnitude of the background, which is nulled or subtracted by the data acquisition software. A computer is used to acquire and store these signals along with the wavelength information, which together yield the spectrum. Although all the measurements reported here are taken at room temperature, the fact that luminescence at low temperature does not present a problem in the DCPR measurement scheme has already been demonstrated earlier.⁹⁻¹¹

IV. RESULTS AND DISCUSSION

Figure 4(a) shows the PR spectrum of a semi-insulating InP sample using a He-Ne laser (632.8 nm) as the pump beam while Fig. 4(b) shows the WLPR spectrum of the same sample. Figure 4(c) shows the pump beam spectrum in the WLPR case, where the shaded region is the part of the spectrum having photons with energy higher than the band gap of InP, which generate electron-hole pairs and modulate the surface electric field in the sample. The incident pump beam power in the WLPR experiment is equal to the area under the shaded region and is about 0.56 mW, while in the PR experiment a 4 mW He-Ne laser is used. This explains the reduced signal strength of the WLPR spectrum. The two features seen in these spectra correspond to the E_0 (band gap) and $E_0 + \Delta_0$ (spin-orbit split-off gap) transitions of InP. By fitting Aspnes' third derivative functional form (TDF⁴) line-shape function to these band-edge features in the PR spectrum, we have estimated the E_0 energy and the associated phenom-

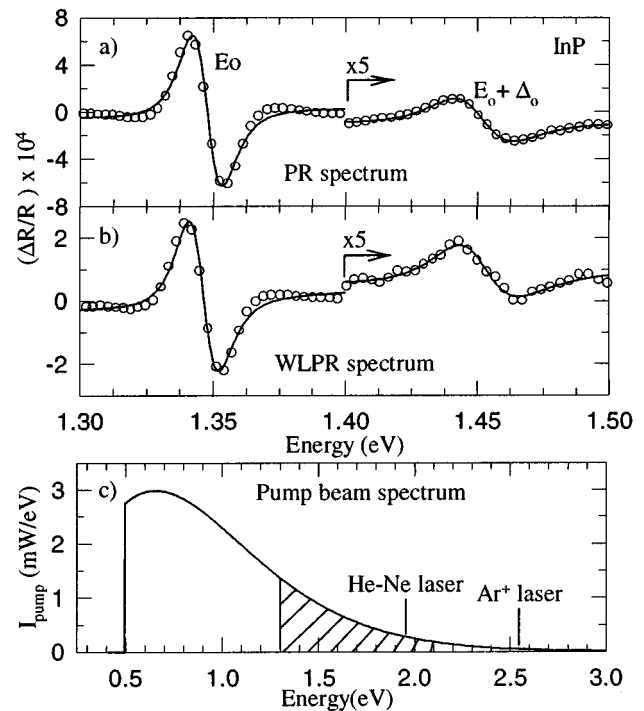


FIG. 4. (a) Conventional PR spectrum of a semi-insulating InP sample using a He-Ne laser (632.8 nm) pump beam. (b) WLPR spectrum of the same sample. The circles are data points and the lines are theoretical fits. (c) The spectrum of the pump beam in the WLPR experiment, the shaded part is strongly absorbed by InP. The photon energies of the He-Ne and Ar⁺ lasers are also indicated.

logical broadening parameter to be 1.347 eV and 11.6 meV, while from the WLPR spectrum these are estimated to be 1.346 eV and 11.6 meV, respectively. Similarly for the $E_0 + \Delta_0$ transitions, these quantities are found to be 1.45 eV and 23.1 meV from PR and 1.451 eV and 23.5 meV from WLPR. As has been shown above, in the dual chopping scheme the signal strength is reduced by a factor of $1/\pi$ as compared to the conventional single chopping scheme. Also, the additional electronics such as the high Q bandpass filter adds to the noise at the detection frequency $f_1 + f_2$. However, the decrease in the signal-to-noise ratio is not critical, as we have shown above that it is possible to obtain identical information using a white light pump beam in the dual chopping mode as with the laser pump beam in the usual single chopping mode. Note that the part of the pump beam spectrum whose energy lies below the band gap of InP is not useful for generation of free carriers in the sample but it adds to the noise in the measurement when it reaches the detector after being scattered by the sample. The use of a short (wavelength) pass optical filter to cutoff this part of the pump beam can improve the signal-to-noise ratio. It has also been shown that the problem of noise and the consequent longer data averaging times with slower scan speeds in a typical modulation spectroscopy experiment can be effectively dealt with by using Fourier transform based filtering techniques.¹³

In the following two examples we show that WLPR spectroscopy has distinct advantages over the conventional PR spectroscopy in the study of semiconductor heterostruc-

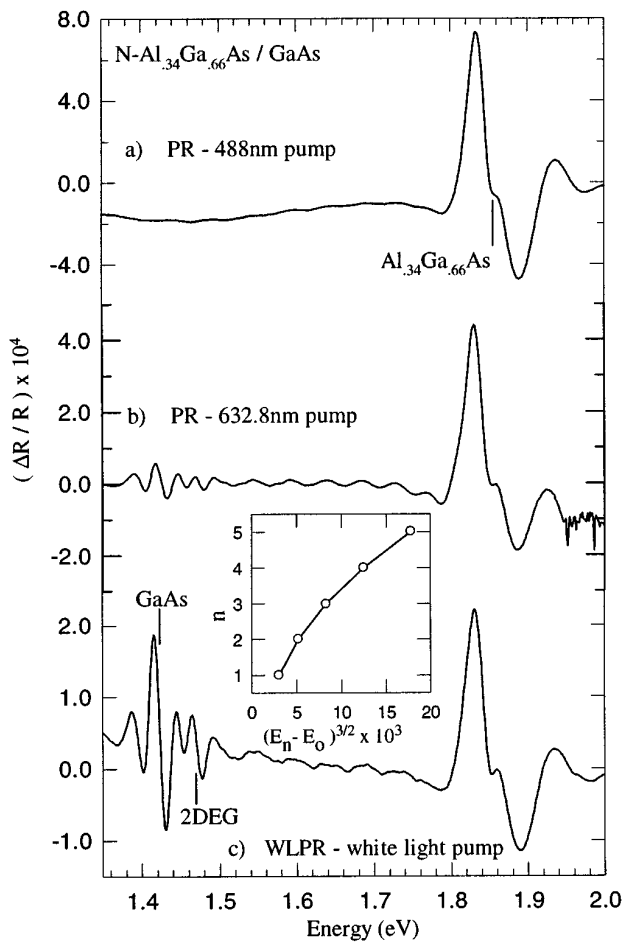


FIG. 5. (a) Conventional PR spectrum of a $N\text{-Al}_{0.34}\text{Ga}_{0.66}\text{As}/\text{GaAs}$ heterostructure sample using an Ar^+ ion laser (488 nm) pump beam. (b) PR spectrum of the same sample using a He-Ne laser (632.8 nm) pump beam. (c) WLPR spectrum of the same sample. The inset shows a plot of the extrema number n of the oscillatory features beyond 1.43 eV in the WLPR spectrum vs $(E_n - E_{0\text{GaAs}})^{3/2}$, E_n = energy at which the extrema occurs. The circles are the data points and the line is a guide to the eye.

tures. Figure 5(a) shows the conventional PR spectrum of a metal-organic chemical-vapor deposition (MOCVD) grown $\text{Al}_x\text{Ga}_{1-x}\text{As}/\text{GaAs}$ heterostructure sample using an Ar^+ laser (488 nm) pump beam. The sample consists of a $3.3 \mu\text{m}$ thick $N\text{-Al}_{0.34}\text{Ga}_{0.66}\text{As}$ layer grown on a n^+ -GaAs substrate with a $0.15 \mu\text{m}$ thick undoped GaAs buffer layer in between. In this spectrum, we see no signature of the underlying GaAs layers. This can happen either due to (i) there being no built-in field at the $\text{Al}_{0.34}\text{Ga}_{0.66}\text{As}/\text{GaAs}$ interface or (ii) the pump beam is completely absorbed by the $\text{Al}_{0.34}\text{Ga}_{0.66}\text{As}$ layer and is not able to reach the $\text{Al}_{0.34}\text{Ga}_{0.66}\text{As}/\text{GaAs}$ interface and generate carriers to modulate the built-in electric field at that interface, while the carriers generated in the $\text{Al}_{0.34}\text{Ga}_{0.66}\text{As}$ layer are also not able to reach that interface to do so. Figure 5(b) shows the conventional PR spectrum of the same sample using a He-Ne laser (632.8 nm) as the pump beam. The part of the $\text{Al}_{0.34}\text{Ga}_{0.66}\text{As}$ spectral feature at energies higher than 1.91 eV is lost because of the use of a 645 nm long (wavelength) pass filter in front of the detector to block the scattered pump beam for reasons explained ear-

lier. Note that had the Al concentration been higher, then its spectrum would have been lost completely. This spectrum also shows a feature at 1.42 eV, which is due to the GaAs layer. The weak oscillatory features at energies below the $\text{Al}_{0.34}\text{Ga}_{0.66}\text{As}$ feature can be identified as arising due to optical interference effects¹⁴ since their periods match those of the oscillatory features seen in the plain reflectance spectrum of this sample. A weak structure is also seen at 1.47 eV. This feature does not look like a continuation of the interference oscillations; however, it is difficult to pinpoint its origin since it virtually merges with the weak interference related oscillatory features. This spectrum, however, shows that out of the two possibilities mentioned above for not being able to see the GaAs feature in the spectrum of Fig. 5(a), the second one is correct. This is because had there been no built-in electric field at the interface we would not have been able to see the GaAs feature at all. Second, the absorption coefficient of $\text{Al}_{0.34}\text{Ga}_{0.66}\text{As}$ being lower at 632.8 nm than at 488 nm, the pump beam is able to penetrate deeper towards the $\text{AlGaAs}/\text{GaAs}$ interface and thereby create charges there to modulate the electric field at that interface. In contrast, the WLPR spectrum of this sample, shown in Fig. 5(c), while simultaneously indicating the presence of both the $\text{Al}_{0.34}\text{Ga}_{0.66}\text{As}$ and the GaAs layers brings out the feature at 1.47 eV quite clearly. This is because in the WLPR experiment, the pump beam photons of energy less than the band-gap energy of $\text{Al}_{0.34}\text{Ga}_{0.66}\text{As}$, but greater than that of GaAs, are able to reach the $\text{Al}_{0.34}\text{Ga}_{0.66}\text{As}/\text{GaAs}$ interface and generate carriers there, and hence, modulate the built-in electric field at that interface to a greater extent than was possible in the earlier two measurements. To identify the feature at 1.47 eV we consider the following. This sample structure is expected to support a two-dimensional electron gas (2DEG) whose signature^{15,16} should lie at energies higher than the GaAs band gap (1.42 eV). This, however, is also the region where one expects to see Franz-Keldysh oscillations (FKO). The inset in Fig. 5 shows a plot of the oscillation extrema number n versus $(E_n - E_{0\text{GaAs}})^{3/2}$. This plot is expected to be linear in the case of FKO,⁴ but in the present case it deviates from linear behavior. Therefore, this structure is most probably the 2DEG signature. Fitting the appropriate line-shape function⁴ to this feature, we find the transition energy to be 1.471 eV from which we estimate the sheet carrier concentration in the 2DEG layer¹⁶ to be $2.9 \times 10^{11} \text{ cm}^{-2}$. Thus, we were able to simultaneously characterize all the layers of the sample. It is evident that more information could be obtained from the WLPR spectrum as compared to the conventional PR spectrum of this sample.

In the next example, we demonstrate selective excitation and probing of semiconductor quantum well interfaces using WLPR. Figure 6(a) shows the conventional PR spectrum of a MOCVD grown $\text{In}_x\text{Ga}_{1-x}\text{As}/\text{GaAs}$ single quantum well (SQW) using a 4 mW He-Ne laser pump beam. The sample consisted of a $\approx 100 \text{ \AA}$ thick $\text{In}_{0.26}\text{Ga}_{0.74}\text{As}$ layer grown on an n^+ -GaAs substrate with an undoped $0.6 \mu\text{m}$ GaAs buffer layer in between and an undoped $0.15 \mu\text{m}$ GaAs cap layer at the top. The transitions corresponding to the various features seen in the spectrum were identified by comparing their energy positions with calculations based on the envelope wave-

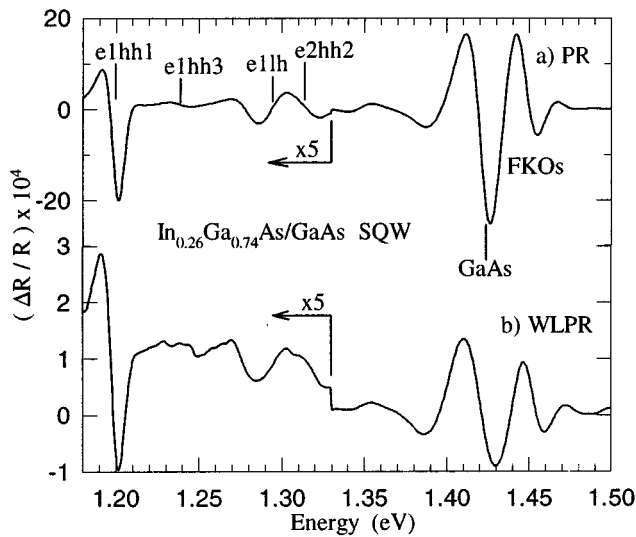


FIG. 6. (a) PR spectrum of a strained $\text{In}_{0.26}\text{Ga}_{0.74}\text{As}/\text{GaAs}$ single quantum well sample using a He–Ne laser (632.8 m) pump beam. The calculated transition energies are indicated by the vertical lines. (b) WLPR spectrum of the same sample but with a InP filter in the pump beam path.

function approximation. Figure 6(b) shows the WLPR spectrum of the same sample, but in this case a polished InP wafer is placed in the pump beam path so that the pump beam spectrum falling on the sample is modified. This modified pump beam spectrum is represented by the unshaded region in Fig. 4(c). A pump beam with such a spectrum cannot generate free carriers in the GaAs ($E_{0\text{GaAs}} = 1.424$ eV) barrier layers and this was experimentally verified by our not being able to obtain a WLPR spectrum of a GaAs sample with this InP filter modified pump beam. Thus, in the WLPR experiment, by generating carriers only in the quantum well (QW), we have selectively modulated the built-in electric field at the $\text{In}_{0.26}\text{Ga}_{0.74}\text{As}/\text{GaAs}$ interface without disturbing the sample surface (air/GaAs), unlike in the PR experiment where this selectivity, using a He–Ne laser, cannot be achieved. It has been suggested earlier^{4,16} that the modulation mechanism, which gives rise to the QW signatures in PR is the pump beam induced periodic changes in the population of the well levels, which affects the QW potential profile (therefore, the electric field), and in turn modifies the eigenstate energies (quantum confined Stark effect). The WLPR spectrum in Fig. 6(b) supports this hypothesis as no free carriers are generated in the bulk GaAs that can modulate the electric field at the heterointerface. The GaAs feature seen in Fig. 6(b) must, therefore, predominantly arise from the $\text{In}_{0.26}\text{Ga}_{0.74}\text{As}/\text{GaAs}$ interface because the electric field in the adjacent barrier layer also gets modulated in the above process, and not from the sample surface (GaAs/air interface). The InP filter modified pump beam has only photons of en-

ergy lower than 1.31 eV, while those below 1.16 eV are not absorbed by the SQW. In this energy range the pump beam has a power ≈ 0.22 mW that is only partially absorbed in the thin SQW layer to generate carriers in the well. On the other hand, in the conventional PR experiment, a much higher number of carriers are generated by the 4 mW He–Ne pump beam being absorbed in the thick GaAs layers. Thus, the field modulation giving rise to the spectrum in Fig. 6(a) is much higher than that in Fig. 6(b). This explains the order of magnitude larger signal strength in Fig. 6(a) as compared to that in Fig. 6(b). The nature of the spectral features is, however, the same in these two measurements. We have estimated the value of the built-in electric field from the FKOs in Fig. 6(b) ($\approx 1.8 \times 10^4$ V cm^{-1}) and found the same value as estimated from the FKOs in Fig. 6(a). This confirms that nearly the same electric field exists at the SQW interfaces as at the air/GaAs interface. We have also calculated the energy levels of the structure using the tunneling resonance technique to solve the Schrödinger equation in the presence of this electric field. We find that a field of this magnitude causes only a minor redshift in the values of the various transition energies.

ACKNOWLEDGMENTS

The authors wish to thank Professor K. L. Narsimhan for his help and encouragement. The authors also thank A. Aziz, V. M. Uplekar, and P. B. Joshi for their assistance.

- ¹J. L. Shay, *Phys. Rev. B* **2**, 803 (1970).
- ²O. J. Glembocki, B. V. Shanabrook, N. Bottka, W. T. Beard, and J. Comas, *Appl. Phys. Lett.* **46**, 970 (1985).
- ³X. Yin and Fred H. Pollak, *Appl. Phys. Lett.* **59**, 2305 (1991).
- ⁴F. H. Pollak and H. Shen, *Mater. Sci. Eng.* **R10**, 275 (1993).
- ⁵H. Shen and M. Dutta, *J. Appl. Phys.* **78**, 2151 (1995).
- ⁶Y. S. Tang, *Phys. Status Solidi A* **129**, 285 (1992).
- ⁷H. Shen, X. C. Shen, F. H. Pollak, and R. N. Sacks, *Phys. Rev. B* **36**, 3487 (1987).
- ⁸M. Sydor, A. Badakhshan, J. R. Engholm, and D. A. Dale, *Appl. Phys. Lett.* **58**, 948 (1991).
- ⁹C. R. Lu, J. R. Anderson, D. R. Stone, W. T. Beard, and R. A. Wilson, *Superlattices Microstruct.* **8**, 155 (1990); C. R. Lu, J. R. Anderson, D. R. Stone, W. T. Beard, R. A. Wilson, T. F. Kuech, and S. L. Wright, *Phys. Rev. B* **43**, 11 791 (1991).
- ¹⁰D. Chandler-Horowitz, D. W. Berning, J. G. Pellegrino, J. H. Burnett, P. M. Amritharaj, D. P. Bour, and D. W. Treat, in *Proceedings of the International Workshop on Semiconductor Characterization*, edited by W. M. Bullis, D. G. Seiler, and A. C. Diebold Inst. Phys. Conf. Ser. (AIP, New York, 1995), p. 639.
- ¹¹S. Ghosh and B. M. Arora, *IEEE J. Sel. Top. Quantum Electron.* **1**, 1108 (1995).
- ¹²J. L. Hilburn, *Manual of Active Filter Design* (McGraw-Hill, New York, 1973).
- ¹³S. Ghosh and B. M. Arora, *Rev. Sci. Instrum.* **68**, 3260 (1997).
- ¹⁴D. Huang, D. Mui, and H. Morkoç, *J. Appl. Phys.* **66**, 358 (1989).
- ¹⁵E. E. Snow, O. J. Glembocki, and B. V. Shanabrook, *Phys. Rev. B* **38**, 12 484 (1988).
- ¹⁶Y. S. Tang, Y. W. Xu, D. S. Jiang, W. H. Zhuang, and M. Y. Kong, *Superlattices Microstruct.* **6**, 391 (1989).